Cooperative long range protein-protein dynamics in Purple Membrane

Maikel C. Rheinstädter[1,2],* Karin Schmalzl[2,3], Kathleen Wood[2,4],† and Dieter Strauch[6]
[1] *Department of Physics and Astronomy, University of Missouri-Columbia, Columbia, MO 65203, U.S.A.*
[2] *Institut Laue-Langevin, 6 rue Jules Horowitz, B.P. 156, F-38042 Grenoble Cedex 9, France*
[3] *Institut für Festkörperforschung, Forschungszentrum Jülich, D-52425 Jülich, Germany*
[4] *Institut de Biologie Structurale Jean Pierre Ebel CEA-CNRS-UJF, F-38027 Grenoble Cedex 1, France and*
[6] *Theoretische Physik, Universität Regensburg, D-93040 Regensburg, Germany*
(Dated: September 28, 2008)

Very recently, interprotein motions in a carboxymyoglobin protein crystal were reported from a molecular dynamics simulation [Phys. Rev. Lett. 100, 138102 (2008)]. We present experimental evidence for a cooperative long range protein-protein interaction in purple membrane (PM). The dynamics was quantified by measuring the spectrum of the acoustic phonons in the 2d Bacteriorhodopsin (BR) protein lattice using inelastic neutron scattering. The data were compared to an analytical model and the effective spring constant for the interaction between protein trimers was determined to be $k = 53.49$ N/m. The experimental results are in very good agreement to the computer simulations, which reported an interaction energy of 1 meV.

PACS numbers: 87.15.km, 87.16.dj, 87.16.D-, 83.85.Hf

The high protein concentration in biological membranes might lead to long-range protein-protein interactions, on which there have been speculations, already some time ago [1]. Recently, interprotein motions in a carboxymyoglobin protein crystal were reported from a molecular dynamics simulation [2, 3]. Motions in proteins occur on various length and time scales [4, 5], and the functional behavior of membrane proteins is likely to depend on the lipid bilayer composition and physical properties, such as hydrophobic thickness and elastic moduli. How the variety of inter- and intra-protein motions, occuring over different time and length scales, interact to result in a functioning biological system remains an open field for those working at the interface of physics and biology. The dynamical coupling between proteins, i.e., *cooperative protein dynamics*, might be important for the understanding of macromolecular function in a cellular context because it might lead to an effective inter-protein communication. Here, we report collective inter-protein excitations in a biological membrane, the purple membrane (PM).

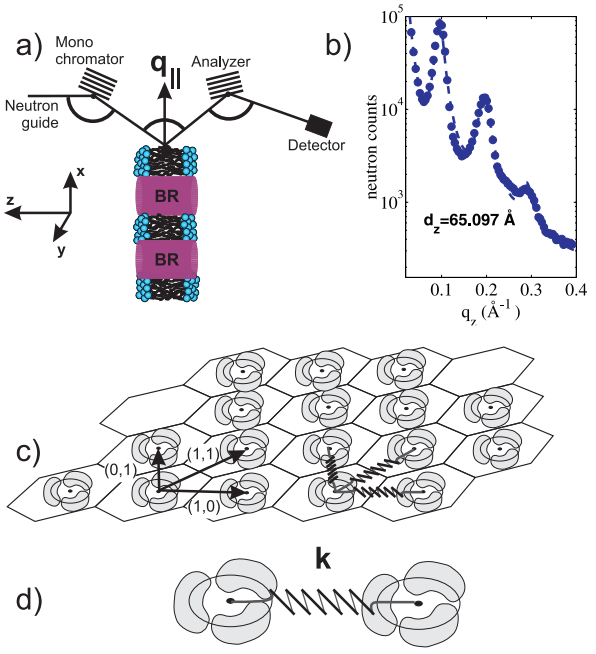

FIG. 1: (Color online). (a) Sketch of the triple-axis scattering geometry. $q_{||}$ is the in-plane component of the scattering vector $\vec{Q}$. (b) Reflectivity curve measured at $T = 30°$C. The dotted line is a fit of Lorentzian peak profiles including a q^{-4} term. (c) BR trimers are arranged on a hexagonal lattice of lattice constant $a \approx 62$ Å. (d) The interaction between the protein trimers is depicted as springs with effective spring constant k.

Purple Membrane (PM) occurs naturally in the form of a two-dimensional crystal, consisting of 75% (wt/wt) of a single protein, Bacteriorhodopsin (BR), that functions as a light-activated proton pump, and 25% various lipid species (mostly phospho- and glyco-lipids) [6]. BR is a proton transporting membrane protein, formed of seven trans-membrane alpha-helices arranged around the photosensitive retinal molecule. The protein in the lipid matrix is organized in trimers that form a highly ordered 2d hexagonal lattice with lattice parameter $a \approx 62$ Å, as depicted in Fig. 1 (c). The structure of PM is well established by electron microscopy, neutron and x-ray diffraction experiments reviewed in [6, 7, 8, 9, 10, 11]. Here we present the unprecedented determination of collective protein–protein dynamics, i.e., acoustic phonons, of the 2d protein lattice in PM using coherent inelastic neutron scattering. The results allowed to determine the effective coupling constant.

The experiments were performed on the IN12 cold-triple-axis spectrometer at the Institut Laue Langevin (ILL, Grenoble, France). IN12 turned out to be highly suited for elastic and inelastic investigations in oriented

biological samples because of its flexibility, good energy resolution and extremely low background. It allows the measurement of diffraction and inelastic scattering in the same run without changing the set-up, which is crucial to assign dynamical modes to structural properties and molecular components. IN12 was equipped with its vacuum box to avoid air scattering at small scattering angles and with vertically focusing monochromator and analyzer to increase the neutron flux at the sample position. There was no horizontal focusing, but the beam was collimated to $40' -$ monochromator $- 30' -$ sample $- 30' -$ analyzer $- 60' -$ detector. All scans were done in W-configuration with fixed $k_f = 1.25$ Å^{-1} resulting in a q resolution of $\Delta q = 0.005$ Å^{-1} and an energy resolution of $\Delta\hbar\omega = 25$ μeV.

Deuterated PM was produced and hydrated by H_2O in order to suppress the contribution of the membrane water to the phonon spectrum in coherent inelastic neutron scattering experiments and to then obtain information on the collective membrane dynamics. Because of the minuteness of the coherent inelastically scattered signals, the preparation of appropriate samples and experimental set-ups is challenging in this type of experiments. We used a completely deuterated PM to enhance the collective protein–protein excitations over other contributions to the inelastic scattering cross section. 200 mgs of deuterated PM suspended in H_2O was centrifuged down and the obtained pellet spread onto a 40×30 mm aluminum sample holder. This was then partially dried to 0.5 g water per gram of membrane over silica gel in a desiccator. The PM patches naturally align along the surface of the sample holder as they dry. The silica gel was then replaced by water, and the sample left to hydrate to a lamellar spacing of $d_z = 65$ Å at 303 K (30°C).

A sketch of the scattering geometry is shown in Fig. 1(a). The experiments were carried out on PM stacks, i.e., PM samples with a regular repeat distance d_z. The mosaicity of the sample (the distribution of normal vectors with respect to the substrate) was checked by rocking scans to about 17 degs. The sample was aligned by centering the first reflectivity Bragg peak at $q_z \approx 0.1$ Å^{-1}. Figure 1(b) shows a reflectivity curve measured at $T = 30$°C. From the three well developed Bragg peaks, the lamellar spacing d_z was determined to be $d_z = 65.1$ Å, corresponding to an average intermembrane water layer of 16 Å, since the thickness of a dry PM fragment is 49 Å. For the inelastic scans, $\vec{Q}$ was placed in the plane of the membranes ($q_{||}$).

The in-plane diffraction pattern of the 2d hexagonal protein lattice was measured and is shown in Fig. 2. Although the normal vectors of the membranes are well aligned with respect to the substrate, the (x, y)-orientation of the membrane layers is statistical and the signal a superposition of the different domains (powder average). All reflections can be indexed by a hexagonal unit cell with a lattice parameter of 61.78 ± 0.73 Å.

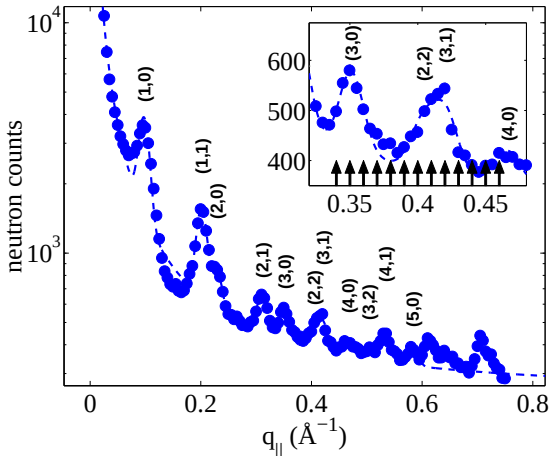

FIG. 2: (Color online). Diffraction pattern of the 2d protein lattice from $q_{||} = 0$ to 0.75 Å^{-1}. The reflections can be indexed by a hexagonal unit cell with a lattice parameter of 61.78 ± 0.73 Å. The dashed line is a fit of the theoretical peak pattern to the data. The inset shows the third Brillouin zone in magnification. The arrows mark the positions of inelastic scans at constant $q_{||}$ values.

Correlations and motions in membranes are often well separated in reciprocal space because of the largely different length and time scales involved. The prominent distances in PM, such as lipid–lipid and BR–BR monomers and trimers for instance lead to spatially well separated signals. The same holds for the different time scales involved from the picosecond (molecular reorientations) to the nano- or microsecond (membrane undulations, large protein motions). The use of oriented samples further allows to separate correlations in the plane of the membranes, and perpendicular to the bilayers. Dynamics between different protein trimers is expected to be dominant where the 2d BR diffraction pattern is observed, i.e., in a $q_{||}$ range of about 0.1 Å^{-1} to 0.6 Å^{-1}. Because elastic and inelastic scattering at small momentum transfers was dominated by the rather strong (1,0) and (1,1) reflections, systematic inelastic scans were taken at $q_{||}$-values in the third Brillouin zone of the 2d pattern, between 0.34 Å^{-1} and 0.46 Å^{-1}. The inset in Fig. 2 shows the Bragg peaks in the third Brillouin zone in magnification and marks the positions of inelastic scans at constant $q_{||}$ values. Figure 3 shows a constant-$q_{||}$ scan at $q_{||} = 0.39$ Å^{-1}. The total inelastic signal typically consists of a Gaussian central peak due to instrumental resolution, quasielastic broadening, which is described by a Lorentzian peak shape, and, for this $q_{||}$ values, two pairs of excitations. Because of the pronounced and symmetric inelastic signals, we are sure that the observed peaks are not spurious effects. The quasielastic signal most likely contains contributions from coherent and incoherent scattering, i.e., from auto- and pair-correlated molecular motions.

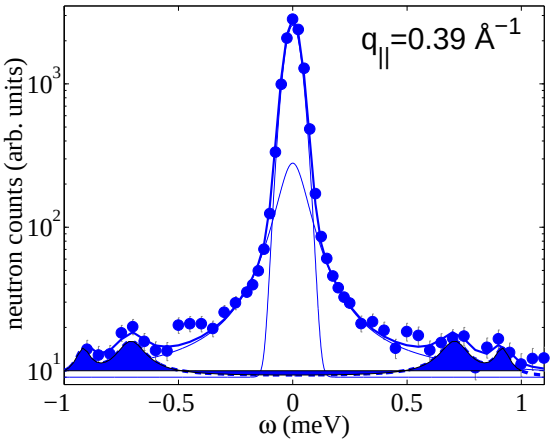

FIG. 3: (Color online). Energy scan at $q_{||} = 0.39$ Å^{-1}. The total inelastic signal consists of a central peak (Gaussian), a Lorentzian quasielastic contribution, and the excitations, described by damped harmonic oscillators.

Propagating modes are experimentally difficult to observe in the scattering function $S(q,\omega)$ as they often show up as a small peak or a soft shoulder in the tails of the central mode and quasielastic broadening, rather than as a clear excitation maximum. In contrast, in the longitudinal spectrum defined by $C_l(q,\omega) = (\omega^2/q^2)S(q,\omega)$, the multiplication by ω^2 suppresses the central mode and quasielastic scattering and makes the excitations (propagating sound modes) more easily visible for analysis. Systematic inelastic scans for $q_{||}$ values between 0.34 Å^{-1} and 0.46 Å^{-1} are shown in Figure 4(a). The position of the Bragg reflections are also marked in the figure.

In order to interpret the data, the excitation spectrum of the 2d protein lattice was modeled analytically. In a simple approach, the protein trimers were taken as the centers of a primitive hexagonal lattice with lattice constant $a = 62$ Å, and the spectrum of the acoustic phonons was calculated. The model is depicted in Fig. 1(c). The basic hexagonal translations are marked by arrows. The interaction between the protein trimers is contained in springs with an effective (longitudinal) spring constant k (Fig. 1(d)). The calculated $C_l(q,\omega)$ is shown in Fig. 4(b). The statistical average leads to a superposition of the different phonon branches, which start and end in the hexagonal Bragg peaks (at $\hbar\omega = 0$). The absolute phonon energies can not be determined from the model, but depend on the coupling constant k. So the energy of the phonon curves in Fig. 4(b) was scaled to match the experiment. Note that because the proteins trimers were treated as dots with an effective mass of M_{tr}, the calculation does not include any contributions from intra-protein or intra-trimer dynamics, i.e., possible optical modes and phonons.

To compare to the data, the most pronounced phonon branches from Figure 4(b) were plotted as solid lines in

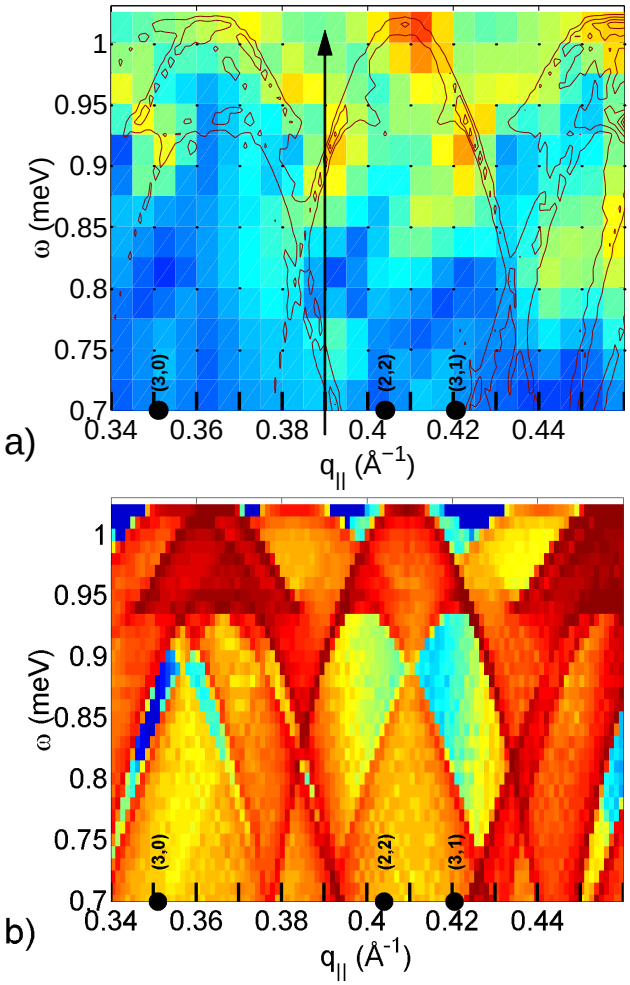

FIG. 4: (Color online). (a) Experimental $C_l(q,\omega)$, measured in the the third Brillouin zone. (b) Calculated excitation spectrum $C_l(q,\omega)$ in the range of the experimental data. The most strongest phonon branches are also shown in part (a) as solid lines.

part (a). In the $q_{||}$ range between 0.34 Å^{-1} and about 0.43 Å^{-1}, the experiment well reproduces the calculated phonon curves. The agreement is less good for $q_{||}$ values above 0.43 Å^{-1}. Only the strongest phonon branches are visible in the data, the weaker branches can most likely not be resolved from the background. The intra-protein dynamics can most likely be observed at higher $q_{||}$ values (because of the smaller distances involved), around the corresponding correlation peaks, and should in a first approximation not interfere with the inter protein dynamics. So it is reasonable to expect that the main structure of the calculated branches is found in the data, but the calculation will not reproduce a possible fine structure due to internal motions. The arrow in Fig. 4(a) marks the position of the energy scan in Fig. 3, at $q_{||} = 0.39$ Å^{-1}. The scan cuts the theoretical dispersion curves twice, at energy values of about $\hbar\omega = 0.7$ meV and $\hbar\omega = 0.9$ meV. The data in Fig. 3

were fitted using two damped harmonic oscillators at $\hbar\omega_0 = \pm 0.71$ meV and $\hbar\omega_0 = \pm 0.92$ meV, in very good agreement to the calculations. It was difficult to observe excitations at energies below about 0.5 meV because of the limited instrumental resolution and the quasielastic scattering contribution. The excitations would then show up as shoulders of the central peak and quasielastic scattering, only, rather than as pronounced inelastic peaks.

Experiment and calculation can be compared to the MD simulations in Ref. [2], where a peak in the energy spectrum at 1 meV was identified as a translational intermolecular protein:protein interaction vibration in a carboxymyoglobin protein crystal. The energy agrees well with the energy of the zone boundary phonon in PM of 1.02 meV, as shown in Fig. 4, but no q-dependence was determined in the computational work. The good agreement of the energy values in the two systems most likely stems from the very high protein density in PM, which makes it almost crystal like. The computational work thus strongly supports the interpretation of our data as collective protein:protein excitations.

The commonly assumed interaction mechanism between inclusions in membranes is a lipid-mediated interaction due to local distortions of the lipid bilayer [12, 13, 14, 15, 16], with a strong dependence on the bilayer properties, in particular elastic properties. The PM might, however, be a special case because there are very few lipids between neighboring BR proteins [17]. While the nature of the interaction still will be mainly elastic, it is not likely to be purely lipid-mediated but for the most part a direct protein–protein interaction. The strength of the interaction can be determined from the data in Fig. 4. The energy of the zone-boundary phonon at the M-point of the hexagonal Brillouin zone (for instance at a $q_{||}$ value of 0.35 Å^{-1}) relates to the coupling constant by $M_{tr}\omega^2 = 6k$. Because this energy is determined as $\hbar\omega = 1.02$ meV, the effective protein–protein spring constant k is calculated to $k = 53.49$ N/m [21]. On the microscopic level, displacing the BR trimer by 1 Å yields a force between neighboring trimers of 5.3 nN. There is therefore strong protein–protein communication in PM. Using the same approach, the spring constant for graphite for comparison is calculated to 27,000 N/m for the in-plane interaction, and 3.5 N/m for out-of-plane interactions. The force constant that we measure in PM thus is 1-2 orders of magnitude larger than the effective van-der-Waals force constant in graphite, but 2-3 orders of magnitude weaker than a C-C bond. The mechanism might be relevant to model the photo cycle in PM where the BR proteins undergo small structural changes [18, 19], which then propagate to neighboring proteins by the coupling k. Because the energy of the excitation is about 1 meV $\approx$ 12 K, this process is highly populated at room temperature (96%) and might therefore be highly relevant for biological function.

In conclusion we present experimental evidence for a cooperative long range protein–protein interaction in purple membrane. The effective spring constant for the interaction between protein trimers can be determined from the acoustic phonon branches as $k = 53.49$ N/m. The finding might be relevant for protein function, i.e., for the photo cycle of BR proteins, where the BR monomers undergo small structural changes. Future experiments will address cooperative intra-protein–trimer and also intra-monomer dynamics. To make a clear relationship to protein function, protein dynamics of activated proteins, i.e., proteins undergoing the photo cycle will be studied.

Acknowledgement: We thank Brigitte Kessler and Dieter Oesterhelt (MPI for Biochemistry, Martinsried) for providing the sample, Martin Weik (IBS, Grenoble) for help with sample preparation, Giuseppe Zaccai (ILL) for critical reading of the manuscript, and the Institut Laue Langevin for the allocation of ample beam time.

* Electronic address: RheinstadterM@missouri.edu
† *Present address:* Biophysical Chemistry, University of Groningen, Nijenborgh 4, 9747 AG Groningen, The Netherlands

[1] R. Lipowsky and E. Sackmann, eds., *Structure and Dynamics of Membranes*, vol. 1 of *Handbook of Biological Physics* (Elsevier, Amsterdam, 1995).
[2] V. Kurkal-Siebert, R. Agarwal, and J. C. Smith, Phys. Rev. Lett. **100**, 138102 (4 pages) (2008).
[3] L. Meinhold, J. C. Smith, A. Kitao, and A. H. Zewail, Proc. Natl. Acad. Sci. U.S.A. **104**, 17261 (2007).
[4] H. Frauenfelder, S. Sligar, and P. Wolynes, Science **254**, 15981603 (1991).
[5] P. Fenimore, H. Frauenfelder, B. McMahon, and R. Young, Proc. Natl. Acad. Sci. U.S.A. **101**, 1440814413 (2004).
[6] U. Haupts, J. Tittor, and D. Oesterhelt, Annu. Rev. Biophys. Biomol. Struct. **28**, 367 (1999).
[7] G. Zaccai, Biophys. Chem. **86**, 249 (2000).
[8] R. Neutze, E. Pebay-Peyroula, E. K., A. Royant, J. Navarro, and E. Landau, Biochim. Biophys. Acta **1565**, 144167 (2002).
[9] J. Lanyi, Annu. Rev. Physiol. **66**, 665 (2004).
[10] I. Koltover, T. Salditt, J.-L. Rigaud, and C. Safinya, Phys. Rev. Lett. **81**, 2494 (1998).
[11] I. Koltover, J. Rädler, T. Salditt, and C. Safinya, Phys. Rev. Lett. **82**, 3184 (1999).
[12] P. A. Kralchevsky, Adv. Biophys. **34**, 25 (1997).
[13] K. Bohinc, V. Kralj-Iglič, and S. May, J. Chem. Phys. **119**, 7435 (2003).
[14] P. Biscari and F. Bisi, Eur. Phys. J. E **6**, 381 (2002).
[15] P. Lagüe, M. J. Zuckermann, and B. Roux, Biophys. J. **81**, 276 (2001).
[16] N. Dan, P. Pincus, and S. Safran, Langmuir **9**, 2768 (1993).
[17] J. Baudry, E. Tajkhorshid, F. Molnar, J. Phillips, and K. Schulten, J. Phys. Chem. **105**, 905 (2001).
[18] A.-N. Bondar, S. Suhai, S. Fischer, J. C. Smith, and M. Elstner, J. Struct. Biol. **157**, 454 (2006).

[19] G. Zaccai, Science **288**, 1604 (2000).
[20] J. F. Hunt, P. D. McCrea, G. Zaccaï, and D. M. Engelman, J. Mol. Biol. **273**, 1004 (1997).
[21] The molecular weight of a BR monomer is 26.9 kDa [20]. Because 1 kg $= 6.0221 \times 10^{26}$ Dalton, the BR trimer thus weighs $m_{tr} = 1.34 \cdot 10^{-22}$ kg